Analytic Inverse Kinematics Considering the Joint Constraints and Self-collision for Redundant 7DOF Manipulator

Jaesung Oh
Department of Mechanical Engineering
Korea Advanced Institute of Science and Technology
Daejeon
ojs9101@kaist.ac.kr

Hyoin Bae
Department of Mechanical Engineering
Korea Advanced Institute of Science and Technology
Daejeon
pos97110@kaist.ac.kr

Jun-Ho Oh
Department of Mechanical Engineering
Korea Advanced Institute of Science and Technology
Daejeon
jhoh@kaist.ac.kr

***Abstract*— This study proposes an analytic inverse kinematic solution considering joint limit and self-collision avoidance for a redundant 7DOF manipulator with spherical shoulder and wrist joints. An analytic approach is used to satisfy the sub-task. The arm angle is used to restrain the manipulator redundancy. The analytic inverse kinematic solution set satisfying the sub-task is proposed by determining the range of the feasible arm angle. The effectiveness of the proposed method was verified through a simulation. We confirmed that the solution of the proposed method always satisfies the joint limit constraints and self-collision avoidance.**

Keywords-component; *Inverse Kinematics, 7DOF Manipulator, Joint Constraints Avoidance, Self-collision Avoidance, Redundant Manipulator*

I. INTRODUCTION

Interest in the role of a robot in an environment, where people cannot be active, has been growing with the development of the robot and artificial intelligence technology. However, the artificial intelligence that would help robots understand their work in certain situations has not yet been developed in environments that include large uncertainty, such as that in the Fukushima nuclear accident.

Tele-operation is mostly used to operate a robot in a disaster environment. However, it is difficult for the operator to know all the information about the robot and the environment and maneuver the robot during these times. Therefore, sub-tasks such as joint limit constraints and self-collision are usually not considered when planning on the robot's motion.

The manipulator redundancy is used to obtain the solution satisfying the sub-task. The manipulator is called the "redundant manipulator" when the degree of freedom (DOF) in the joint space is higher than that in the task space. Therefore, restraining its self-motion to determine the particular solution of the inverse kinematics (IK) is necessary. However, the working efficiency decreases as the operator sets the constraints all the time, considering various information about the robot and the environment.

Accordingly, many studies aimed to find the IK solution of the redundant manipulator to satisfy tasks and sub-tasks, such as joint limit and self-collision avoidance. The DOF of a typical task space is 6DOF, and ensuring a minimum redundancy is possible. Therefore, many studies have been performed on the manipulator with a 7DOF (e.g., human arm).

Many of the studies that discussed the IK problems considering sub-tasks used a numerical approach (NA). The gradient-projection, extended Jacobian, and weighted least-norm methods are usually used in the case of the NA [1–4]. A research based on the Jacobian method has also been performed to satisfy sub-tasks such as joint limit avoidance, manipulability enhancement (singularity avoidance), torque optimization, and obstacle avoidance (self-collision avoidance) using the null space of the manipulator [5–9].

However, the iteration process to converge the solution is necessary in the NA. The accuracy and calculation time of the solution have a trade-off relationship.

Therefore, studies are actively conducted to calculate the analytic solution for the IK problem and overcome the disadvantage of the NA. Most of these studies use the arm angle parameter to restrain the manipulator redundancy [10–16]. The arm angle is the angle between a certain reference plane and the plane, including the shoulder, elbow, and wrist [10]. Several methods can be used to define a reference plane. One method is to define the reference plane as the plane including a certain fixed vector [10, 11, 14, 16]. Another is to define the reference plane as the sagittal plane, including the z-axis in the global coordinate and vector connecting the shoulder and wrist [12–13]. Another parameter (e.g., dual-arm angle, which is a modified arm angle) is used to prevent algorism singularity when determining the reference plane

978-1-5090-6724-4/17 $31.00 © 2017 IEEE
DOI 10.1109/IRC.2017.46

IEEE computer society

[11]. Studies satisfying the sub-task using an analytic approach are also conducted. The representative study aims to obtain the analytic IK solution of the 7DOF manipulator considering the joint limit constraints [15–16]. However, compared with the numerical approach, the analytic solution of the IK considering the variable sub-task has not been proposed yet. Therefore, Kiréanski and Ananthanarayanan used both analytic and numerical approaches to obtain a solution that would satisfy the desired task and sub-task [17–18]. However, some disadvantages also existed, including the fact that the accuracy and intuition are lower than those for the completely analytic solution.

We propose herein the analytic solution of the IK for the 7DOF redundancy manipulator with a spherical shoulder and wrist joint that can consider two sub-tasks: joint limit and self-collision avoidance. The feasible range of the arm angle is calculated using the proposed method. The median value of the range is finally selected to calculate the IK.

Section 2 introduces the forward and inverse kinematics for a model of the manipulator used in the research. The method to efficiently setup the reference plane of the arm angle is also proposed. Section 3 presents the methods to obtain the feasible range of the arm angle to consider the self-collision and joint limit.

II. Forward and Inverse Kinematics of the Manipulator

Figure 1 shows the structure of the robot to be handled in this paper. The structure presents the robot body and the manipulator. The manipulator has 7DOF, including the rotating elbow joint and the spherical shoulder and wrist joints. Table 1 shows the parameter of the manipulator expressed using the DH parameter.

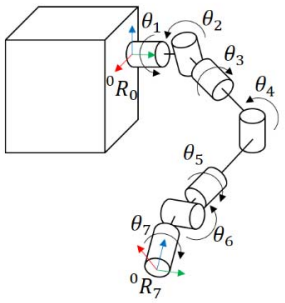

Figure 1. Robot body and 7DOF manipulator with spherical shoulder and wrist joints. The global coordinate is the center of the shoulder. The orientation is the same with body orientation.

The forward and inverse kinematics of the 7DOF manipulator are analytically represented by setting the arm angle, which restrains the 1DOF because the task space is 6DOF. Equation (1) is a general homogeneous transform matrix comprising a translation matrix and a rotation matrix (i.e., Tr and Rt, respectively).

$$ {}^{n-1}T_n = \mathrm{Tr}_{z_{n-1}}(d_n)Rt_{z_{n-1}}(\theta_n)Tr_{x_n}(a_n)Rt_{x_n}(\alpha_n) \quad (1) $$

Table 1. Denavit-Hartenberg (DH) parameters of the 7DOF manipulator

	d_n	θ_n	a_n	α_n
0	0	0	0	$-\pi/2$
1	d_{bs}	$\theta_1 + \pi/2$	0	$\pi/2$
2	0	$\theta_2 - \pi/2$	0	$\pi/2$
3	0	$\theta_3 + \pi/2$	0	$-\pi/2$
4	$-d_{se}$	θ_4	0	$\pi/2$
4’	$-d_{ew}$	0	0	0
5	0	θ_5	0	$-\pi/2$
6	0	θ_6	0	$\pi/2$
7	0	θ_7	0	0
7’	$-d_{wt}$	0	0	0

A. Manipulator Kinematics

When setting the base coordinate to center of shoulder, d_{bs} is zero. The position and orientation of the end-effector are represented by (2) and (3), respectively.

$$ {}^0x_7 = {}^0R_3\{ {}^3l_{se} + {}^3R_4({}^4l_{ew} + {}^4R_7\, {}^7l_{wt})\} \quad (2) $$

$$ {}^0R_7 = {}^0R_3\, {}^3R_4\, {}^4R_7 \quad (3) $$

l_{se} is the vector from the shoulder to the elbow. l_{ew} is the vector from the elbow to the wrist of the robot. l_{wt} is the vector from the wrist to the tip of the end-effector. It is the general expression of the 7-DOF manipulator forward kinematics.

B. Inverse Kinematics of the Manipulator [10, 11, 14, 16]

We preferentially calculated the reference rotation matrix ${}^0R_3^o$, which included ${}^0l_{se}^o$ on the reference plane, to determine the IK solution considering the arm angle. After that, ${}^0R_\psi$ was applied to ${}^0R_3^o$. ${}^0R_\psi$ is the rotation matrix used to rotate the amount of the arm angle along the ${}^0u_{sw}$ axis.

$$ {}^0R_3 = {}^0R_\psi\, {}^0R_3^o \quad (4) $$

$$ {}^0R_\psi = I_3 + sin\psi\,[\,{}^0u_{sw}\times] + (1 - cos\psi)[\,{}^0u_{sw}\times]^2 \quad (5) $$

$$ [u\times] = \begin{bmatrix} 0 & -u_3 & u_2 \\ u_3 & 0 & -u_1 \\ -u_2 & u_1 & 0 \end{bmatrix} \quad (6) $$

Several methods are used to set the reference plane. However, in this paper, we set the plane, including the z-axis of the global coordinate and ${}^0x_{sw}$.

Using ${}^0R_3$, θ_1 , θ_2 , and θ_3 were represented by (9)–(11), respectively. Equation (4) can be rewritten as (7) by using (5). Equation (8) is obtained from Table 1.

$$\begin{gathered} {}^0R_3 = {}^0R_\psi \, {}^0R_3^o = \mathrm{A}_s sin\psi + B_s cos\psi + C_s \\ \mathrm{A}_s = \left[{}^0u_{sw} \times \right] {}^0R_3^o \\ B_s = -\left[{}^0u_{sw} \times \right]^2 {}^0R_3^o \\ C_s = \left[{}^0u_{sw} \, {}^0u_{sw}^T \right] {}^0R_3^o \end{gathered} \tag{7}$$

$${}^0R_3 = \begin{bmatrix} * & * & s\theta_1 c\theta_2 \\ c\theta_2 s\theta_3 & c\theta_2 c\theta_3 & -s\theta_2 \\ * & * & c\theta_1 c\theta_2 \end{bmatrix} \tag{8}$$

$$\tan\theta_1 = \frac{a_{s13} sin\psi + b_{s13} cos\psi + c_{s13}}{a_{s33} sin\psi + b_{s33} cos\psi + c_{s33}} \tag{9}$$

$$\sin\theta_2 = -a_{s23} sin\psi - b_{s23} cos\psi - c_{s23} \tag{10}$$

$$\tan\theta_3 = \frac{a_{s21} sin\psi + b_{s21} cos\psi + c_{s21}}{a_{s22} sin\psi + b_{s22} cos\psi + c_{s22}} \tag{11}$$

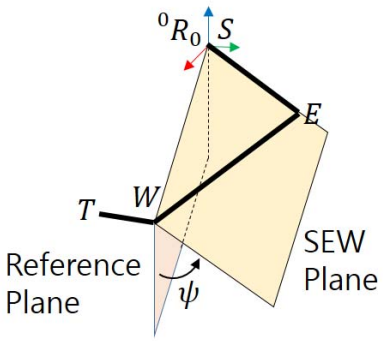

Figure 2. Definition of the arm angle, ψ. The reference plane includes the z-axis in the global coordinate and ${}^0x_{sw}$. The SEW plane includes the shoulder (S), elbow (E), and wrist (W).

Accordingly, θ_4 is represented using the cosine formula by (12) because it is one of the angles of the SEW triangle. $\mathrm{d_{se}}$ and $\mathrm{d_{ew}}$ are the length of the links, and $\mathrm{d_{sw}}$ is the length of shoulder to wrist.

$$\cos\theta_4 = \frac{d_{sw}^2 - d_{se}^2 - d_{ew}^2}{2 d_{se} d_{ew}} \tag{12}$$

$$d_{sw} = \left| {}^0x_7^d - {}^0R_7^d \, {}^7l_{wt} \right| \tag{13}$$

Using the ${}^4R_7$, θ_5 , θ_6 , and θ_7 are represented by (16)–(18), respectively.

$${}^4R_7 = A_w sin\psi + B_w \cos\psi + \mathrm{C_w} \tag{14}$$

$$\begin{gathered} \mathrm{A_w} = {}^3R_4^T A_s^T \, {}^0R_7^d \\ \mathrm{B_w} = {}^3R_4^T B_s^T \, {}^0R_7^d \\ \mathrm{C_w} = {}^3R_4^T C_s^T \, {}^0R_7^d \end{gathered}$$

$${}^4R_7 = \begin{bmatrix} * & * & c\theta_5 s\theta_6 \\ * & * & s\theta_5 s\theta_6 \\ -s\theta_6 c\theta_7 & s\theta_6 s\theta_7 & c\theta_6 \end{bmatrix} \tag{15}$$

$$\tan\theta_5 = \frac{a_{w23} sin\psi + b_{w23} cos\psi + c_{w23}}{a_{w13} sin\psi + b_{w13} cos\psi + c_{w13}} \tag{16}$$

$$\cos\theta_6 = a_{w33} sin\psi + b_{w33} cos\psi + c_{w33} \tag{17}$$

$$\tan\theta_7 = \frac{a_{w32} sin\psi + b_{w32} cos\psi + c_{w32}}{-a_{w31} sin\psi - b_{w31} cos\psi - c_{w31}}. \tag{18}$$

Thus, expressing all joint angles is possible by arm angle, except the elbow axis, which can be organized into tangent and cosine forms.

C. Reference Plane of the Arm Angle

The sagittal plane herein included the z-axis of the global coordinate and ${}^0x_{sw}$.

${}^0R_3^o$ is represented by (24) because of the geometrical characteristic. The sine formula was used to calculate θ of (19). θ is the angle between two vectors (i.e., ${}^0l_{sw}$ and ${}^0l_{se}$). ${}^0x_{sw}$ and ${}^0l_{se}$ were on the reference plane when rotated by ${}^0R_3^o$. $\vec{\mathrm{u}}_\mathrm{x}$, $\vec{\mathrm{u}}_\mathrm{y}$, and $\vec{\mathrm{u}}_\mathrm{z}$ are the orthonormal vectors composing the reference rotation matrix, ${}^0R_3^o$.

$$\vec{\mathrm{u}}_\mathrm{z} = - {}^0R_\theta \vec{\mathrm{u}}_\mathrm{sw} \tag{19}$$

$$\theta = \sin^{-1}\left(\frac{d_{ew}}{d_{sw}} \sin q_4 \right) \tag{20}$$

$$\vec{\mathrm{u}}_\mathrm{sw} = \frac{{}^0x_{sw}}{\left| {}^0x_{sw} \right|} \tag{21}$$

$$\vec{\mathrm{u}}_\mathrm{y} = \begin{cases} \left[-\dfrac{\alpha u_{sw,y}}{u_{sw,x}} \quad \alpha \quad 0 \right]^T & \text{where } \vec{u}_{sw,x} \neq 0 \\ [0 \quad 1 \quad 0]^T & \text{where } \vec{u}_{sw,x} = 0 \end{cases} \tag{22}$$

$$\alpha = \frac{u_{sw,x}}{\sqrt{u_{sw,x}^2 + u_{sw,y}^2}}$$

$$\vec{\mathrm{u}}_\mathrm{x} = \vec{u}_y \times \vec{\mathrm{u}}_\mathrm{z} \tag{23}$$

$${}^0R_3^o = \left[\vec{u}_x \; \vec{u}_y \; \vec{u}_z \right] \tag{24}$$

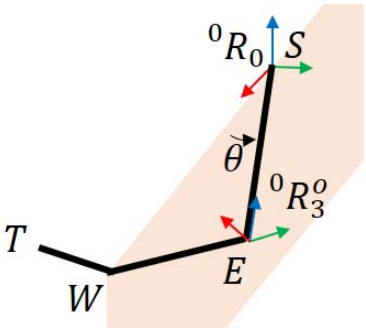

Figure 3. Reference plane and reference rotation matrix. The z-axis of the reference rotation matrix is always on the reference plane.

The sagittal plane included the z-axis in the global coordinate and is selected without additional parameters (e.g., dual-arm angle) when determining $\vec{u}_y$. We can avoid algorithm singularity if we use the proposed reference plane under the case that the global z-axis and $^0l_{sw}$ are parallel.

III. Proposed Feasible Range of the Arm Angle

As discussed in Section 2, finding the analytic IK solution of the 7DOF manipulator was possible by limiting the arm angle. Therefore, we can obtain the range of the arm angle using the previous research to avoid the joint limit [16]. In addition to this method, the range of the arm angle was also proposed herein to avoid self-collision and joint limit.

A. Feasible range of the arm angle to avoid self-collision

As shown in Figure 4, we can check the collision between the robot body and the manipulator when the robot is projected on a global x–y global coordinate plane. Therefore, we can confirm whether or not the collision between the robot and upper arm occurs if we find the plane containing the global z-axis and $^0u_{se}$, which is the unit vector of $^0l_{se}$.

The parameters comprising the plane were calculated by using (26) and (27). $^0l_{se}$ was defined by the arm angle from (2) similar to (25).

$$\begin{aligned} {}^0u_{se} &= {}^0R_3\ {}^3u_{se} \\ &= A_s\ {}^3u_{se} sin\psi + B_s\ {}^3u_{se} \cos\psi + C_s\ {}^3u_{se} \\ &= \mathrm{A}'_s sin\psi + B'_s cos\psi + \mathrm{C}'_s \\ \mathrm{A}'_s &= A_s\ {}^3u_{se}, B'_s = \mathrm{B}_s\ {}^3u_{se}, \mathrm{C}'_s = C_s\ {}^3u_{se} \end{aligned} \tag{25}$$

$$\begin{aligned} \vec{h}_1 &= {}^0u_{se} \times \vec{z} = [-[0\ 0\ 1]^T \times]\ {}^0u_{se} \\ &= \begin{bmatrix} a'_2 sin\psi + b'_2 \cos\psi + c'_2 \\ -a'_1 sin\psi - b'_1 \cos\psi - c'_1 \\ 0 \end{bmatrix} \end{aligned} \tag{26}$$

$$\mathrm{d}_1 = -\vec{h}_1 \cdot {}^0l_{bs} \tag{27}$$

$\vec{h}_1$ is the normal vector, and d_1 is the scalar parameter of the plane, including the global z-axis and the unit vector of $^0l_{se}$. $\vec{h}_1$ can be calculated using the cross product of $^0u_{se}$ and $\vec{z}$ because it is orthonormal with both vectors. d_1 is calculated by using the dot product of the normal vector of the plane and a vector on the plane. The center of the shoulder of the robot is always on the plane. Therefore, we use $^0l_{bs}$ to calculate d_1 in this study. We can set the inequality condition using $\vec{h}_1$ and d_1 to avoid the collision between the robot body and the upper arm of the manipulator similar to (28).

$$\vec{\mathrm{h}}_1 \cdot {}^0l_{ch} + d_1 > 0 \tag{28}$$

$$\begin{aligned} \alpha_1 sin\psi + \alpha_2 cos\psi + \alpha_3 > 0 \\ \alpha_1 = \mathrm{a}'_2 l_{ch,x} - a'_1 l_{ch,y} \\ \alpha_2 = \mathrm{b}'_2 l_{ch,x} - b'_1 l_{ch,y} \\ \alpha_3 = \mathrm{c}'_2 l_{ch,x} - c'_1 l_{ch,y} \end{aligned} \tag{29}$$

The feasible range of the arm angle avoiding the self-collision between the robot body and the upper arm was represented by (29) if the edge of the convex hull composing the robot body was $^0l_{ch}$. Therefore, confirming the collision by the arm angle was possible using this method.

Even though we avoid the collision between the robot body and the upper arm, the collision between the lower arm and the robot body becomes possible. We can then calculate the range of the arm angle using the same process to avoid the collision between the lower arm and the robot body represented by (34).

$$\begin{aligned} {}^0u_{ew} &= \mathrm{A}''_s sin\psi + B''_s cos\psi + \mathrm{C}''_s \\ \mathrm{A}''_s &= A_s\ {}^3R_4\ {}^4u_{ew} \\ \mathrm{B}''_s &= B_s\ {}^3R_4\ {}^4u_{ew} \\ \mathrm{C}''_s &= C_s\ {}^3R_4\ {}^4u_{ew} \end{aligned} \tag{30}$$

$$\begin{aligned} \vec{h}_2 &= {}^0u_{ew} \times \vec{z} = [-[0\ 0\ 1]^T \times]\ {}^0u_{ew} \\ &= \begin{bmatrix} a''_2 sin\psi + b''_2 \cos\psi + c''_2 \\ -a''_1 sin\psi - b''_1 \cos\psi - c''_1 \\ 0 \end{bmatrix} \end{aligned} \tag{31}$$

$$\begin{aligned} \mathrm{d}_2 &= -\vec{\mathrm{h}}_2 \cdot {}^0x_{sw} \\ &= -(\mathrm{a}''_2 x_{sw,x} - a''_1 x_{sw,y}) sin\psi - (\mathrm{b}''_2 x_{sw,x} - b''_1 x_{sw,y}) cos\psi \end{aligned} \tag{32}$$

$$\vec{\mathrm{h}}_2 \cdot {}^0l_{ch} + d_2 > 0 \tag{33}$$

$$\begin{aligned} \beta_1 sin\psi + \beta_2 cos\psi + \beta_3 > 0 \\ \beta_1 = \mathrm{a}''_2 l_{ch,x} - a''_1 l_{ch,y} - \mathrm{a}''_2 x_{sw,x} + a''_1 x_{sw,y} \\ \beta_2 = \mathrm{b}''_2 l_{ch,x} - b''_1 l_{ch,y} - \mathrm{b}''_2 x_{sw,x} + b''_1 x_{sw,y} \\ \beta_3 = \mathrm{c}''_2 l_{ch,x} - c''_1 l_{ch,y} \end{aligned} \tag{34}$$

Therefore, self-collision can be avoided if the arm angle to satisfy (29) and (34) was used.

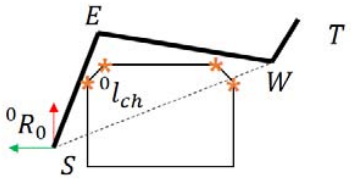

Figure 4. Self-collision avoidance strategy using the arm angle. ${}^0l_{ch}$ is the edge of the convex hull and the given information

B. Feasible range of the arm angle to avoid the joint limit constraint

The method proposed by Shimizu was used to calculate the range of the arm angle to avoid the joint limit [16]. The joint angle according to the arm angle can be expressed by tangent and cosine forms as (35) and (37). The arm angle according to the joint angle can be expressed by (39) in reverse.

$$\tan\theta_i = \frac{a_n sin\psi + b_n \cos\psi + c_n}{a_d sin\psi + b_d cos\psi + c_d} \tag{35}$$

$$\begin{gathered} \mathrm{A}\sin\psi + \mathrm{B}\cos\psi + \mathrm{C} = 0 \\ A = \mathrm{a_d} tan\theta_i - a_n, \mathrm{B} = \mathrm{b_d} tan\theta_i - b_n, \mathrm{C} = \mathrm{c_d} tan\theta_i - c_n \end{gathered} \tag{36}$$

$$\cos\theta_i = asin\psi + bcos\psi + c \tag{37}$$

$$\begin{gathered} \mathrm{A}\sin\psi + \mathrm{B}\cos\psi + \mathrm{C} = 0 \\ \mathrm{A} = \mathrm{a}, \mathrm{B} = \mathrm{b}, \mathrm{C} = c - cos\theta_{i.} \end{gathered} \tag{38}$$

Equation (36) and (38) can be easily summarized as (39) by using the substitution rule as follows:

$$\begin{gathered} \psi = 2\tan^{-1}\frac{-\mathrm{B}' \pm \sqrt{B'^2 - 4A'C'}}{2A'} \text{ where } \mathrm{B}'^2 - 4A'C' \geq 0 \\ \mathrm{A}' = C - B, \mathrm{B}' = 2A, \mathrm{C}' = \mathrm{C} + \mathrm{B} \end{gathered} \tag{39}$$

The feasible range of the arm angle that satisfied the limits of each joint was determined using the abovementioned function and joint limit values.

Therefore, the median value of the biggest continuous range of the arm angle among the intersections with the range of the arm angle was selected for the desired arm angle to ensure the joint limit and self-collision avoidance. Moreover, simultaneously avoiding the joint limit and self-collision was possible.

IV. Simulation

The link parameter and joint limit constraints of the manipulator were set at the same value of the DRC-HUBO+ for a realistic simulation. However, the link offset of the elbow joint herein was ignored to simplify the equation.

Table 2. Joint limit constraints of DRC-HUBO+. The unit used is degree.

Joint	1	2	3	4	5	6	7
Lower limit	−180	−30	−120	−160	−135	−90	−180
Upper limit	180	180	90	30	135	90	180

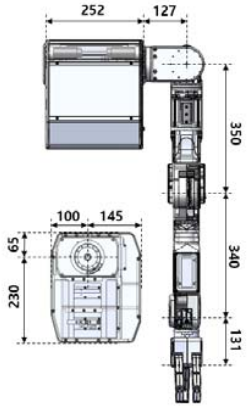

Figure 5. Length parameter of DRC-HUBO+. The unit used is millimeter.

The edges of the convex hull composing the robot body are presented as follows when the base coordinate is the center of the shoulder.

$$\begin{gathered} {}^0l_{ch1} = [100, -127, 65]^T \\ {}^0l_{ch2} = [100, -379, 65]^T \end{gathered}$$

The desired task is as follows:

$$\begin{gathered} {}^0x_d = [150, -600, -200]^T \\ {}^0R_d = \begin{bmatrix} 0.866 & 0 & -0.500 \\ 0.500 & 0 & 0.866 \\ 0 & -1 & 0 \end{bmatrix} \end{gathered}$$

The feasible range of the arm angle to satisfy (29) and (34), which are for the self-collision avoidance, is as follows:

$$\begin{gathered} \psi_{\mathrm{ch1,sw}} = [26.1755, 130.9110] \\ \psi_{\mathrm{ch2,sw}} = [18.5307, 170.8435] \\ \psi_{\mathrm{ch1,we}} = [3.8536, 172.4385] \\ \psi_{\mathrm{ch2,we}} = [27.8070, 166.1444] \end{gathered}$$

The feasible range of the arm angle for joint limit avoidance is as follows:

$$\begin{gathered} \psi_2 = [0, 58.6659] \\ \psi_3 = [0, 96.6932] \\ \psi_7 = [0, 61.2965] \\ \psi_{\mathrm{i}} = [0, 180], \text{where } i = 1, 5, 6 \end{gathered}$$

The intersection of the two feasible ranges of the arm angle depending on each constraint is as follows:

$$\psi = [27.8070, 58.6659]$$

The median value ψ^* of the feasible range to the arm angle was finally selected. The IK solution can be calculated using ψ^*.

$$\psi^* = 43.2365$$
$$\theta^* = [-35.8, -28.0, -98.4, -78.9, -42.1, 47.3, 168.3]^T$$

Therefore, we confirm that all joint angles satisfy the joint limit constraints. We also conclude the absence of a self-collision with the robot body and the manipulator. Even though the robot body has two edges of convex hull (i.e., ${}^0l_{ch1}$ and ${}^0l_{ch2}$), the manipulator configuration determined from the proposed inverse kinematic solution avoids the robot body (Figure 6).

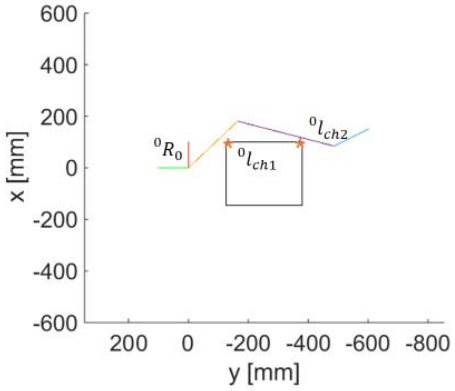

Figure 6. Simulation result of the proposed method. The convex hull has two edges. The simulation parameters are the same with those of DRC-HUBO+.

V. Conclusion

This study proposed a method to determine the feasible range of the arm angle to achieve joint limit and self-collision avoidance. The arm angle was used to restrain the self-motion of the redundant manipulator with spherical shoulder and wrist joints.

The simulation result confirmed the joint limit and self-collision avoidance when the arm angle belonged to the feasible range. The simulation was conducted by using realistic parameters, such as the link lengths and joint limit values of DRC-HUBO+. Directly applying the proposed IK solution to the realistic robots was possible.

However, this paper did not consider the case of collision between the robot body and end-effector and the link offset of the elbow joint.

Therefore, in future, we will conduct a research applying the proposed IK solution to the manipulator with the link offset of the elbow joint. We will also consider the collision between the robot body and the end-effector.

References

[1] Dubey, R. V., Euler, J. A., & Babcock, S. M. (1991). Real-time implementation of an optimization scheme for seven-degree-of-freedom redundant manipulators. IEEE Transactions on Robotics and Automation, 7(5), 579-588.

[2] Shah, M., & Patel, R. V. (2005). Inverse jacobian based hybrid impedance control of redundant manipulators. In IEEE International Conference Mechatronics and Automation, 2005 (Vol. 1, pp. 55-60). IEEE.

[3] Huang, L. G., & Li, Y. (1997, July). Repeatable kinematic control of redundant manipulators: Implementation issues. In Advanced Robotics, 1997. ICAR'97. Proceedings., 8th International Conference on (pp. 147-152). IEEE.

[4] Xiang, J., Zhong, C., & Wei, W. (2010). General-weighted least-norm control for redundant manipulators. IEEE Transactions on Robotics, 26(4), 660-669.

[5] Nenchev, D. N. (1989). Redundancy resolution through local optimization: A review. Journal of robotic systems, 6(6), 769-798.

[6] Yoshikawa, T. (1985, March). Manipulability and redundancy control of robotic mechanisms. In Robotics and Automation. Proceedings. 1985 IEEE International Conference on (Vol. 2, pp. 1004-1009). IEEE.

[7] Suh, K. C., & Hollerbach, J. M. (1987). LOCAL VERSUS GLOBAL TORQUE OPTIMIZATION OF REDUNDANT MANIPULATORS. In IEEE.

[8] Nakamura, Y., Hanafusa, H., & Yoshikawa, T. (1987). Task-priority based redundancy control of robot manipulators. The International Journal of Robotics Research, 6(2), 3-15.

[9] Nenchev, D. N., Tsumaki, Y., & Takahashi, M. (2004). Singularity-consistent kinematic redundancy resolution for the SRS manipulator. In Intelligent Robots and Systems, 2004.(IROS 2004). Proceedings. 2004 IEEE/RSJ International Conference on (Vol. 4, pp. 3607-3612). IEEE.

[10] Kreutz-Delgado, K., Long, M., & Seraji, H. (1992). Kinematic analysis of 7-DOF manipulators. The International journal of robotics research, 11(5), 469-481.

[11] Yan, L., Mu, Z., & Xu, W. (2014, October). Analytical inverse kinematics of a class of redundant manipulator based on dual arm-angle parameterization. In2014 IEEE International Conference on Systems, Man, and Cybernetics (SMC)(pp. 3744-3749). IEEE.

[12] Cui, Z., Pan, H., Qian, D., Peng, Y., & Han, Z. (2012, August). A novel inverse kinematics solution for a 7-DOF humanoid manipulator. In 2012 IEEE International Conference on Mechatronics and Automation.

[13] An, H. H., Clement, W. I., & Reed, B. (2014, July). Analytical inverse kinematic solution with self-motion constraint for the 7-DOF restore robot arm. In 2014 IEEE/ASME International Conference on Advanced Intelligent Mechatronics (pp. 1325-1330). IEEE.

[14] Yu, C., Jin, M., & Liu, H. (2012, August). An analytical solution for inverse kinematic of 7-DOF redundant manipulators with offset-wrist. In 2012 IEEE International Conference on Mechatronics and Automation (pp. 92-97). IEEE.

[15] Wang, L. C., & Chen, C. C. (1991). A combined optimization method for solving the inverse kinematics problems of mechanical manipulators. IEEE Transactions on Robotics and Automation, 7(4), 489-499.

[16] Shimizu, M., Kakuya, H., Yoon, W. K., Kitagaki, K., & Kosuge, K. (2008). Analytical inverse kinematic computation for 7-DOF redundant manipulators with joint limits and its application to redundancy resolution. IEEE Transactions on Robotics, 24(5), 1131-1142.

[17] Kiréanski, M. V., & Petrović, T. M. (1993). Combined analytical-pseudoinverse inverse kinematic solution for simple redundant manipulators and singularity avoidance. The International journal of robotics research, 12(2), 188-196.

[18] Ananthanarayanan, H., & Ordóñez, R. (2015). Real-time Inverse Kinematics of (2n+ 1) DOF hyper-redundant manipulator arm via a combined numerical and analytical approach. Mechanism and Machine Theory, 91, 209-226.